

ODE-GS: Latent ODEs for Dynamic Scene Extrapolation with 3D Gaussian Splatting

Daniel Wang¹ Patrick Rim¹ Tian Tian² Alex Wong¹ Ganesh Sundaramoorthi³

¹Yale University ²RISD ³RTX

¹{daniel.wang.dhw33, patrick.rim, alex.wong}@yale.edu

²ttian@risd.edu ³ganesh.sundaramoorthi@rtx.com

Abstract

We present **ODE-GS**, a novel method that unifies 3D Gaussian Splatting with *latent* neural ordinary differential equations (ODEs) to forecast dynamic 3D scenes far beyond the time span seen during training. Existing neural rendering systems—whether NeRF- or 3DGS-based—embed time directly in a deformation network and therefore excel at *interpolation* but collapse when asked to predict the future, where timestamps are strictly out-of-distribution. ODE-GS eliminates this dependency: after learning a high-fidelity, time-conditioned deformation model for the training window, we freeze it and train a Transformer encoder that summarizes past Gaussian trajectories into a latent state whose continuous evolution is governed by a neural ODE. Numerical integration of this latent flow yields smooth, physically plausible Gaussian trajectories that can be queried at any future instant and rendered in real time. Coupled with a variational objective and a lightweight second-derivative regularizer, ODE-GS attains state-of-the-art extrapolation on D-NeRF and NVFI benchmarks, improving PSNR by up to 10 dB and halving perceptual error (LPIPS) relative to the strongest baselines. Our results demonstrate that continuous-time latent dynamics are a powerful, practical route to photorealistic prediction of complex 3D scenes.

1 Introduction

The ability to predict the future evolution of dynamic 3D scenes is essential for intelligent systems, enabling applications such as autonomous navigation, augmented reality, and embodied AI. This task involves two key challenges: (1) forecasting dense motion trajectories to capture the temporal dynamics of scene elements, and (2) rendering these predicted states from arbitrary viewpoints with high fidelity. While recent advancements in computer vision and robotics have made strides toward addressing these challenges, seamlessly integrating motion forecasting with photorealistic rendering for extrapolation beyond observed timestamps remains an open problem. Overcoming this gap is critical for real-time predictive perception in complex, time-evolving environments.

Neural rendering techniques, notably Neural Radiance Fields (NeRF) [24], have transformed novel view synthesis by enabling high-quality 3D scene reconstruction from sparse image sets. These methods have impacted fields such as robotics [16], depth estimation [15], and surface reconstruction [39], due to their photorealistic rendering capabilities. Subsequent to NeRF as an alternative radiance field representation, 3D Gaussian Splatting [18] offers real-time rendering efficiency while maintaining visual quality, accelerating progress in dynamic scene modeling. By explicitly representing scene elements as Gaussian primitives, this approach facilitates efficient visualization of time-evolving environments, such as objects in motion within videos.

However, most existing dynamic scene models, such as Deformable 3D Gaussians [38] and 4D Gaussian Splatting [36], focus on interpolation—predicting scene states within the observed temporal range (e.g., estimating the scene at $t = 3$ given frames at $t = 1, 2, 4$). These methods leverage time-conditioned deformation fields to achieve smooth temporal transitions within the training window $[t_{\min}, t_{\max}]$, and can achieve high-quality results while modeling accurate dynamics within the defined temporal range of the training samples. However, such time-conditioned models face a critical generalization hurdle when extrapolating to unseen time: future timestamps are, by definition, out-of-distribution from a temporal perspective. These models tend to overfit the specific sequence of dynamics present in the training data. Consequently, when tasked with predicting beyond this familiar temporal horizon, their lack of explicit mechanisms for modeling the underlying principles of long-term motion leads to poor performance. This inability to generalize temporally restricts their utility in real-world applications that demand robust prediction of future states.

Many dynamic scenes exhibit recurring motion patterns, such as periodic movements or object oscillations, suggesting that extrapolation is feasible by learning from past trajectories. Building on this insight, we propose a novel framework that extends 3D Gaussian Splatting [18] to forecast future scene states. Our approach models Gaussian parameters (position, rotation, and scale) as trajectories in a continuous-time latent space, leveraging the efficiency of Gaussian Splatting for both motion prediction and rendering.

Unlike time-conditioned models that rely on explicit timestamp inputs, our method employs a Transformer-based Latent Ordinary Differential Equation (ODE) model, inspired by continuous-time forecasting techniques [5]. This model auto-regressively predicts future Gaussian parameters based solely on observed trajectory histories, avoiding generalization issues associated with time-dependent functions. By formulating the latent dynamics as an ODE, solved via numerical integration, we ensure smooth, physically plausible motion trajectories that can be sampled at arbitrary future timestamps. This continuous-time approach contrasts with discrete-step autoregressive models like GaussianPrediction [41], offering greater temporal smoothness and flexibility critical for high-fidelity 3D scene forecasting.

Our framework operates in two stages: Stage 1 optimizes a canonical Gaussian set and a deformation MLP for interpolation within the observed time window, following [38]. Stage 2 freezes these components and trains a Transformer-Latent ODE to extrapolate Gaussian trajectories, combining trajectory-based losses with optional rendering losses for visual refinement. This design leverages the explicit spatial representation of Gaussian Splatting and the temporal continuity of ODEs to achieve robust extrapolation and high-quality rendering.

Our contributions are:

- We propose a novel framework integrating 3D Gaussian Splatting with a Transformer-based Latent ODE for dynamic scene extrapolation, enabling high-fidelity forecasting of future states from past Gaussian trajectories.
- We formulate Gaussian parameter dynamics using an ODE-based latent space, solved via numerical integration, to achieve smooth and coherent motion trajectories adaptable to arbitrary future times.
- We demonstrate the effectiveness of our approach through extensive experiments on two dynamic scenes datasets, showcasing significantly better extrapolation performance and rendering quality compared to existing dynamic 3D scene prediction methods.

2 Related Works

2.1 Novel View Synthesis

Recent advances in scene reconstruction and free-viewpoint rendering have explored a diverse range of approaches, including explicit mesh-based representations [3, 7, 25, 26], and implicit neural volume representations [22]. Among these, Neural Radiance Fields (NeRF) [24] have emerged as a dominant paradigm due to their ability to synthesize photorealistic novel views, particularly in static scenes. The foundational success of NeRF has led to numerous extensions for dynamic scene reconstruction [1, 8, 27, 28, 31], enabling applications such as monocular video-based scene reconstruction [12, 21, 35], editable scene representations [17, 28], and human-centered reconstructions [30, 29]. Furthermore,

efforts to improve the efficiency of NeRF-based methods have resulted in significant advancements in fast rendering and reconstruction techniques [4, 10, 11, 13, 33, 34].

2.2 Dynamic Scene Modeling with 3D Gaussians

3D Gaussian Splatting [18] (3DGS) has emerged as a powerful technique, combining swift reconstruction and rendering speeds with exceptional quality, initially for static scenes but increasingly adapted for dynamic contexts. Deformable 3D Gaussians [38] learn Gaussians in a canonical space with a deformation network. By training both the canonical Gaussians and the deformation network simultaneously, they enable continuous-time rendering by transforming canonical Gaussians into arbitrary time within the training window. Concurrently, 4D Gaussian Splatting [36] took the same canonical-deform strategy and additionally integrated 4D neural voxels inspired by HexPlane [4]. Additional efforts, such as explicit time-variant Gaussian features [23], demonstrate exceptional qualities in dynamic scene modeling, achieving interactive frame rates and enabling flexible editing like object insertions. However, most 3DGS-based approaches rely on a time-conditioned deformation field, making these models exceptional in interpolation tasks but unable to extrapolate into unseen time in the future. GaussianPrediction [41] has recently explored this issue by combining a superpoint strategy with Graph Convolution Networks (GCN) that directly conditions on past motion instead of time, but is only capable of sampling at discrete steps when extrapolating. GaussianVideo [2] has also combined Neural-ODE with hierarchical Gaussian splatting, although they mainly focused on using ODE for learning smooth camera trajectories rather than scene motion, and was also designed for interpolation tasks. Currently, we are the only work that predicts scene dynamics via novel view synthesis with continuous time.

2.3 Neural Ordinary Differential Equations

Neural Ordinary Differential Equations (Neural ODEs) [5] introduced a novel approach for continuous-depth neural networks. Instead of defining discrete layers, a Neural ODE specifies the continuous dynamics of a hidden state using a neural network that parameterizes its derivative. The network’s output is then determined by a numerical ODE solver that integrates these learned dynamics over a specified interval. Key advantages include memory-efficient training via the adjoint sensitivity method, inherent handling of irregularly-sampled data, and adaptive computation.

Relevant to dynamic modeling, Latent ODEs [32] typically encode an input sequence into an initial latent representation whose continuous-time evolution is then governed by a Neural ODE. A decoder can subsequently map these evolving latent states back to the observation space at arbitrary times. This is powerful for modeling continuous trajectories and is often combined with Variational Autoencoders (VAEs), as in ODE2VAE [40], to learn distributions over latent paths and capture uncertainty. Our work shares this philosophy of modeling dynamics in a latent space via an ODE but emphasizes autoregressive prediction from past trajectories.

The synergy between recurrent methods and Neural ODEs has also been explored. For instance, GRU-ODE [6] adapts GRU-like gating mechanisms to continuously evolving states, while ODE-RNN [32] interleaves discrete RNN updates at observation points with continuous ODE-based evolution between them. These hybrid models effectively capture both event-driven and continuous aspects of time series.

Further research has focused on enhancing Neural ODEs. Augmented Neural ODEs (ANODEs) [9] improve expressive power by expanding the state space. For more efficient and stable training, Heavy Ball Neural ODEs (HBNODEs) [37] incorporate momentum into the continuous dynamics, and advancements like algebraically reversible solvers [14] offer exact gradient computation with constant memory cost. These developments underscore the ongoing efforts to refine Neural ODEs for complex dynamic modeling tasks.

3 Method

Our method models dynamic 3D scenes through a two-stage framework. Stage 1 optimizes canonical 3D Gaussians and a deformation network that maps them to observed timestamps, learning to interpolate within the training window. Stage 2 freezes these components and trains a Transformer-based Latent ODE model that takes sequences of Gaussian trajectories as input. The Transformer

encodes observed trajectories into a latent state, which is then evolved forward through a neural ODE to predict future states. These evolved latent states are decoded back to Gaussian parameters and rendered using standard Gaussian Splatting. By learning from trajectory sequences rather than absolute timestamps, the model extrapolates beyond the observed time range while maintaining temporal continuity through the ODE dynamics.

3.1 Problem Definition

Formally, we define our task as follows: given a dataset of calibrated RGB images capturing a dynamic 3D scene:

$$\mathcal{D} = \{(I_i, V_i, t_i)\}_{i=0}^N, \quad I_i : \Omega \rightarrow \mathbb{R}^3, \quad V_i \in SE(3), \quad t_i \in \mathbb{R}, \quad (1)$$

we learn a continuous-time rendering operator $\mathcal{F}_\Theta : \mathbb{R} \times SE(3) \rightarrow (\Omega \rightarrow \mathbb{R}^3)$ that generates RGB images for any time t and camera pose V . The operator decomposes as:

$$\mathcal{F}_\Theta(t, V) = \mathcal{R}(\mathcal{G}_\Theta(t), V), \quad \mathcal{G}_\Theta(t) = \begin{cases} \bar{\mathcal{G}} + \mathcal{D}_\omega(t, \bar{\mathcal{G}}) & \text{if } t_{\min} \leq t \leq t_{\max}, \\ \mathcal{E}_\phi(\mathcal{S}, t) & \text{if } t > t_{\max}, \end{cases} \quad (2)$$

where $\bar{\mathcal{G}} = \{\bar{G}_k\}_{k=1}^M$ is a canonical set of 3D Gaussians, \mathcal{D}_ω is an interpolation deformation function, \mathcal{E}_ϕ is our extrapolation function, and \mathcal{R} is the differentiable rasterizer from [18]. Each canonical Gaussian $\bar{G}_k = (\mu_k, R_k, S_k, c_k, \alpha_k)$ comprises geometric parameters $(\mu_k, R_k, S_k) \in \mathbb{R}^{10}$ (position $\mu_k \in \mathbb{R}^3$, rotation R_k from unit quaternion, and scale S_k diagonal matrix) and appearance parameters (c_k, α_k) (spherical harmonics coefficients and opacity). The deformation functions \mathcal{D}_ω and \mathcal{E}_ϕ modify only the geometric parameters, while appearance parameters remain fixed after initial optimization. View-dependent color is computed as $C_k(V) = \sum_{l=0}^L \sum_{m=-l}^l c_k^{l,m} Y_l^m(V)$, and covariance is $\Sigma_k = R_k S_k S_k^\top R_k^\top$.

The differentiable rasterizer \mathcal{R} renders images by projecting each 3D Gaussian onto the image plane, computing per-pixel alpha compositing with front-to-back blending:

$$C(p) = \sum_{k \in \mathcal{N}(p)} c_k \alpha_k \prod_{j=1}^{k-1} (1 - \alpha_j), \quad (3)$$

where $\mathcal{N}(p)$ are Gaussians affecting pixel p , c_k is the color, and α_k is the opacity after 2D projection. Our two-stage approach first learns $\bar{\mathcal{G}}$ and \mathcal{D}_ω for interpolation (Trajectory Initialization), then freezes these components and trains \mathcal{E}_ϕ for extrapolation using generated Gaussian trajectories $\mathcal{S} = \{\bar{\mathcal{G}} + \mathcal{D}_\omega(t_i, \bar{\mathcal{G}})\}_{i=0}^T$.

Our strategy decomposes the problem into two distinct stages, a design choice that allows us to first focus on accurately representing the observed scene dynamics before learning to forecast them. This separation simplifies the learning task at each stage. In stage 1, we aim to learn the canonical 3D Gaussians $\bar{\mathcal{G}}$ as well as the interpolation deformation model \mathcal{D}_ω . Then in stage 2, we use the previously learned \mathcal{D}_ω to generate the sequence \mathcal{S} and train the \mathcal{E}_ϕ for extrapolation.

3.2 Time-Conditioned Interpolation Model (Stage 1)

In this stage, we learn a model for scene interpolation by adopting the methodology of Deformable 3D Gaussians [38]. The scene’s dynamics are represented by deforming a static set of canonical 3D Gaussians, $\bar{\mathcal{G}}$. This deformation is driven by a small, time-conditioned MLP, \mathcal{D}_ω , which learns to predict geometric offsets for position, rotation, and scale for each Gaussian based on a given timestamp t . Both the canonical set $\bar{\mathcal{G}}$ and the deformation network are optimized jointly by minimizing a photometric loss (L1 + D-SSIM) against the training images within the observed time window.

The primary purpose of this stage is to function as a high-fidelity generator for the dynamic trajectories that will be used to train our extrapolation model. After convergence, we freeze the parameters of both the canonical Gaussians $\bar{\mathcal{G}}$ (including their optimized appearance) and the deformation network \mathcal{D}_ω . This frozen model is then used to generate sequences of historical Gaussian parameters, $\mathcal{S} = \{\bar{\mathcal{G}} + \mathcal{D}_\omega(t_j, \bar{\mathcal{G}})\}_{j=0}^{T_{obs}-1}$, which serve as the direct input for the second stage.

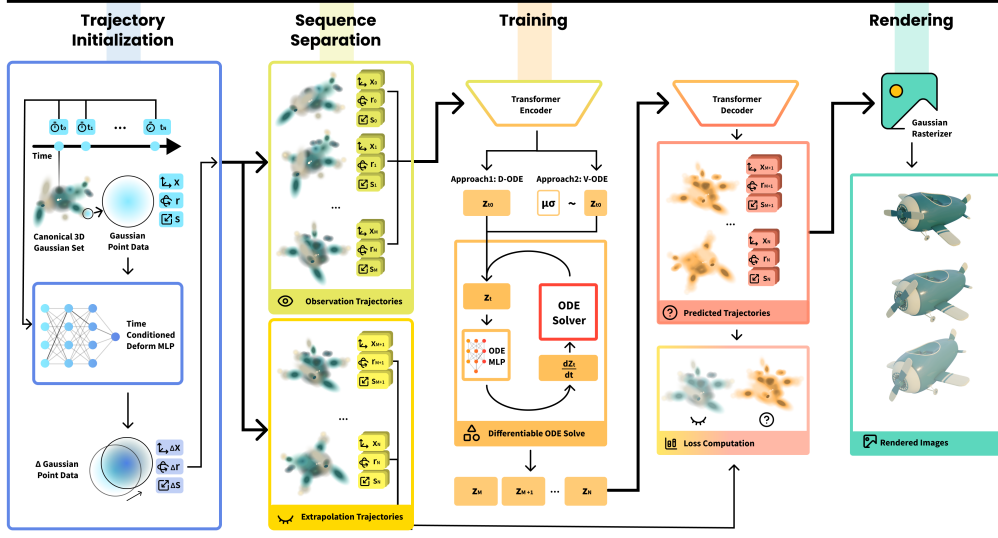


Figure 1: Overview of ODE-GS. 1: Trajectory Initialization learns a canonical set of 3D Gaussians and a lightweight time-conditioned deformation MLP that exactly interpolates the training window, yielding dense per-Gaussian trajectories. 2: Sequence Separation slices each trajectory into an observed prefix (input) and a held-out suffix (supervision) to mimic test-time forecasting. 3: Latent-ODE Training encodes the observed prefix with a Transformer, infers a latent initial state, and evolves it forward with a neural ODE; a decoder maps the latent path back to Gaussian parameters, which are matched to ground-truth suffixes via trajectory and optional rendering losses, regularised by a second-derivative smoothness term. 4: Rendering passes predicted Gaussians through the real-time rasterizer of [18], enabling photorealistic, continuous-time novel-view extrapolation.

3.3 Dynamic Sequence Separation for Trajectory Training

With the continuous interpolation model from Stage 1—comprising the frozen canonical set $\bar{\mathcal{G}}$ and deformation network \mathcal{D}_ω —we leverage it as a generative oracle to create a robust training dataset for the Stage 2 extrapolation task, \mathcal{E}_ϕ . The key to this process is that we are no longer restricted to the original training timestamps. We fully exploit the continuous nature of our learned function by querying the model to produce geometric parameters $x_k(t)$ for any arbitrary, real-valued time $t \in [t_{\min}, t_{\max}]$. This capability allows us to implement a dynamic sequence separation strategy where we create a vast dataset of training samples. Each sample consists of an observation sequence, $\mathcal{S}_{obs} = \{x_k(t_j)\}_{j=0}^{T_{obs}-1}$, and its corresponding future ground-truth sequence, $\mathcal{S}_{target} = \{x_k(t_j)\}_{j=T_{obs}}^{T_{obs}+T_{extrap}-1}$. To ensure the forecasting model generalizes well and does not overfit to a fixed cadence, training batches are deliberately constructed to contain a rich diversity of these trajectories, featuring different starting times and temporal spans. This stage effectively translates the continuous representation from Stage 1 into the varied, sequential input-output pairs $(\mathcal{S}_{obs}, \mathcal{S}_{target})$ required to train the Latent ODE model in Stage 2, which learns to predict \mathcal{S}_{target} given \mathcal{S}_{obs} .

3.4 Time-Independent Latent ODE Model For Extrapolation (Stage 2)

With the interpolation model ($\bar{\mathcal{G}}$ and \mathcal{D}_ω) learned and frozen, the second stage focuses on training the extrapolation function \mathcal{E}_ϕ introduced in Section 3.1. The goal is to predict future scene states $\mathcal{G}_\Theta(t) = \mathcal{E}_\phi(\mathcal{S}, t)$ for times $t > t_{\max}$, based on observed historical Gaussian parameter trajectories \mathcal{S} . As illustrated in Figure 1, \mathcal{E}_ϕ is realized by a Transformer-based Latent Ordinary Differential Equation (ODE) model. This model is designed to learn the underlying continuous-time dynamics from sequences of past geometric parameters (position, rotation, and scale) of the Gaussians.

The input to this stage consists of sequences $\mathcal{S}_k = \{x_k(t_j)\}_{j=0}^{T_{obs}-1}$ for each Gaussian k , where $x_k(t_j)$ represents its geometric parameters. The Transformer-based Latent ODE model, \mathcal{E}_ϕ , comprises a Transformer encoder, a latent ODE (f_θ), and a decoder (δ_ψ). This architecture autoregressively predicts future parameters from observed histories, avoiding explicit time conditioning to improve generalization. The core of our extrapolation model is a variational latent ODE, chosen to account for the inherent stochasticity of future scene dynamics. We detail this approach below.

3.4.1 Probabilistic Forecasting with a Variational Latent ODE

Even when conditioned on an observed past trajectory, the future evolution of a dynamic scene can be inherently stochastic. For example, an object might follow one of several plausible paths. A purely deterministic model would be forced to predict an average, likely unrealistic, future. To account for this uncertainty, our primary approach models the future trajectory distribution using a Variational Latent ODE (V-ODE), inspired by [32].

Variational Inference and Dynamics. Instead of mapping the observed history to a single initial state for the ODE, we infer a probability distribution over possible initial states. The Transformer encoder processes the historical trajectory \mathcal{S}_k for a Gaussian k into a context vector h_k . A projection head then outputs the parameters of a Gaussian posterior distribution, $q_\phi(z_k(t_0) | \mathcal{S}_k) = \mathcal{N}(\mu_{z_k}, \text{diag}(\sigma_{z_k}^2))$, for the initial latent state $z_k(t_0)$ at the beginning of the extrapolation window. During training, we sample from this distribution using the reparameterization trick: $z_k(t_0) = \mu_{z_k} + \sigma_{z_k} \odot \epsilon$, $\epsilon \sim \mathcal{N}(0, I)$.

This sampled latent state $z_k(t_0)$ is then evolved forward in time by numerically solving the latent ODE, $z_k(t) = \text{ODESolve}(f_\theta, z_k(t_0), t)$. Finally, the decoder δ_ψ maps the latent trajectory $z_k(t)$ back to the predicted Gaussian geometric parameters $\hat{x}_k(t)$.

Objective. The V-ODE model is trained by maximizing the Evidence Lower Bound (ELBO), which corresponds to minimizing the following loss:

$$\mathcal{L}_{\text{V-ODE}} = \lambda_{\text{pred}} \sum_{t \geq t_{T_{\text{obs}}}} \underbrace{[-\log p_\sigma(x_k(t) | \hat{x}_k(t))]}_{\text{prediction NLL}} + \lambda_{\text{kl}} \text{KL}[q_\phi(z_k(t_0) | \mathcal{S}_k) \parallel p(z_k(t_0))] + \lambda_{\text{reg}} \mathcal{R}_{\text{sm}} \quad (4)$$

The loss consists of three components: a negative log-likelihood (NLL) term that encourages the predicted trajectory to match the ground truth, a Kullback-Leibler (KL) divergence term that regularizes the latent space by keeping the posterior close to a unit Gaussian prior $p(z_k(t_0))$, and our smoothness regularizer \mathcal{R}_{sm} (Sec. 3.4.2).

Deterministic Variant. As a simpler baseline, we also consider a deterministic version of the model (D-ODE). In this variant, the encoder directly outputs a single point estimate for the initial latent state, $z_k(t_0) = g(h_k)$. Consequently, the KL divergence term is removed from the loss, and the prediction loss becomes a direct L1 distance: $\mathcal{L}_{\text{D-ODE}} = \lambda_{\text{pred}} \sum_{t \geq t_{T_{\text{obs}}}} \|x_k(t) - \hat{x}_k(t)\|_1 + \lambda_{\text{reg}} \mathcal{R}_{\text{sm}}$. While computationally simpler, this deterministic approach lacks the capacity to model the multi-modal nature of future predictions.

3.4.2 Second Derivative Regularization

A naïvely trained latent ODE can over-fit short observed windows and subsequently extrapolate with unphysical high-frequency oscillations. To mitigate this, we introduce a lightweight yet effective regularizer that *directly* penalizes the *second* temporal derivative of the latent flow field.

Let $\{t_\ell\}_{\ell=0}^K$ be the timestamps at which the ODE is evaluated and $\dot{z}_\ell = f_\theta(z(t_\ell))$ be the instantaneous velocity of the latent state computed by the ODE function f_θ . We approximate the latent acceleration by a first-order finite difference and define the regularization term \mathcal{R}_{sm} as the mean squared magnitude of this approximate acceleration:

$$\mathcal{R}_{\text{sm}} = \frac{1}{K-1} \sum_{\ell=1}^{K-1} \left\| \frac{\dot{z}_\ell - \dot{z}_{\ell-1}}{t_\ell - t_{\ell-1}} \right\|_2^2. \quad (5)$$

Intuitively, this enforces C^2 smoothness in the latent trajectory, discouraging jerky movements without overly damping legitimate long-range trends and adding minimal computational overhead.

4 Experiments

In this section, we evaluate the effectiveness of our proposed framework, which we refer to as ODE-GS (Ordinary Differential Equation-based Gaussian Splatting), for extrapolating dynamic 3D scenes. We begin by detailing our implementation and the datasets used in Section 4.1. We then present quantitative results in Section 4.2 to assess rendering quality on unseen future timestamps across multiple datasets, followed by qualitative evaluations in Section 4.3 to demonstrate visual coherence and realism.

4.1 Implementation Details and Datasets

4.1.1 Model Architecture

The Transformer encoder uses $d_{\text{model}} = 128$ dimensions with $n_{\text{head}} = 8$ attention heads and $L_{\text{enc}} = 5$ encoder layers. For the latent ODE component, we set the latent dimension to $d_{\text{latent}} = 64$ and use an MLP with $L_{\text{ode}} = 4$ layers and $d_{\text{hidden}} = 64$ hidden units per layer. The decoder network mirrors this structure with $L_{\text{dec}} = 5$ layers and $d_{\text{hidden}} = 128$ hidden units. For the ODE function, we use Tanh activations for smooth and bounded outputs.

4.1.2 Training Procedure

Our training is implemented as a two-stage process with PyTorch and integrates with the original 3D Gaussian Splatting renderer [18]. For solving ODEs, we use the `torchode` package [19] with its adaptive DOPRI5 solver configured with tolerances $rtol = 10^{-3}$ and $atol = 10^{-4}$. We train our models on NVIDIA GPUs (RTX 3090 or A6000) with a batch size of 512 for 40 epochs. We apply an initial learning rate of 4×10^{-4} for the primary phase, dynamically adjusted using a Cosineannealing scheduler with a minimum learning rate of 1×10^{-6} by the end of training.

For variational training, we use an initial noise standard deviation of $\sigma = 10^{-3}$ and gradually anneal the KL divergence weight from 0.01 to 0.1 over the first 20 epochs to prevent posterior collapse. The regularization loss weight is set to $\lambda_{\text{reg}} = 10^{-3}$. The curriculum learning strategy (Section ??) uses an observation time span of $T_{\text{obs}} = 0.3$, initial extrapolation span of $\tau_{\text{init}} = 0.0$, maximum extrapolation span of $\tau_{\text{max}} = 0.3$, 20 observation points (N_{obs}), 20 extrapolation points (N_{extrap}), a curriculum multiplier of $\mu = 2.0$, and a base stage duration of 5 epochs.

4.1.3 Testing Procedure

For testing extrapolation performance of the model, we select the last segment of the training data time that is the same length as the observed time in training. The Stage 1 deformation MLP \mathcal{D}_{ω} generates the corresponding Gaussian parameter trajectories $\mathcal{W}_k = \{x_k(t_i)\}_{i=N-N_{\text{obs}}}^N$ for each Gaussian k , where $x_k(t_i) = x_{k,c} + \mathcal{D}_{\omega}(t_i, \mu_{k,c})$. These trajectories are fed into the Transformer encoder f_{enc} to produce the initial latent state $z_k(t_N)$.

The Latent ODE f_{θ} is then solved forward in time using the ODE solver (e.g., Dormand-Prince with adaptive step size) to generate the latent trajectory $z_k(t)$ for all validation timestamps $t \in \{t_{N+1}, \dots, t_{\text{max}}\}$. The decoder δ_{ψ} maps these latent states to predicted Gaussian parameters $\hat{x}_k(t) = \delta_{\psi}(z_k(t))$. The predicted parameters are rendered using the Gaussian Splatting rasterizer \mathcal{R} to produce images $\hat{\mathcal{I}}(t) = \mathcal{R}(\mathcal{G}(t), \mathcal{V}_t)$, where $\mathcal{G}(t) = \{\hat{x}_k(t)\}_{k=1}^M$ and \mathcal{V}_t is the camera viewpoint at time t . We compute evaluation metrics (PSNR, SSIM, LPIPS) by comparing $\hat{\mathcal{I}}(t)$ to the ground-truth images $\mathcal{I}(t)$, providing a comprehensive assessment of visual quality and temporal coherence.

4.1.4 Datasets

We evaluate ODE-GS on two datasets: the D-NeRF dataset [31] and the NVFI dataset [20]. The D-NeRF dataset comprises eight synthetic dynamic scenes (Lego, Mutant, Standup, Trex, Jumpingjacks, Bouncingballs, Hellwarrior, Hook), each containing 100-200 training images and 20 test images with timestamps normalized from 0 to 1, rendered at 800×800 resolution with black backgrounds to isolate object motion dynamics. The NVFI dataset provides two subcategories: the simpler Dynamic Object Dataset featuring rotating objects (fan, whale, shark, bat, telescope) and the more challenging Dynamic Indoor Scene Dataset (chessboard, darkroom, dining, factory) containing multi-object

Table 1: Quantitative extrapolation results on the D-NeRF dataset. Metrics reported include PSNR, SSIM, and LPIPS-vgg (higher PSNR/SSIM, lower LPIPS-vgg is better). The best metric is highlighted in bold, and the second best is underlined.

Scene	TiNeuVox-B			4D-GS			Deformable-GS			GaussianPredict			Ours Det.			Ours Var.		
	PSNR ↑	SSIM ↑	LPIPS ↓	PSNR ↑	SSIM ↑	LPIPS ↓	PSNR ↑	SSIM ↑	LPIPS ↓	PSNR ↑	SSIM ↑	LPIPS ↓	PSNR ↑	SSIM ↑	LPIPS ↓	PSNR ↑	SSIM ↑	LPIPS ↓
Lego	23.34	.9102	.0942	24.25	.9150	.0810	23.25	.9349	.0579	12.25	.7594	.2325	<u>25.25</u>	.9150	<u>.0578</u>	26.39	.9337	.0565
Mutant	24.40	.9282	.0700	22.48	.9300	.0520	24.45	.9310	.0461	27.12	.9514	<u>.0285</u>	<u>33.66</u>	<u>.9776</u>	.0134	34.04	.9790	.0139
Standup	21.77	.9169	.0927	18.61	.9180	.0840	21.37	.9124	.0844	26.91	.9456	.0465	<u>28.81</u>	<u>.9489</u>	<u>.0406</u>	29.55	.9531	.0361
Trex	20.72	.9284	.0751	23.83	.9460	.0510	20.74	.9421	<u>.0465</u>	21.52	.9443	.0437	20.77	.9407	.0534	<u>21.70</u>	<u>.9453</u>	.0475
Jumpingjacks	19.87	.9115	.0954	19.95	.9270	<u>.0770</u>	20.32	.9162	.0790	20.12	.9150	.0811	22.34	<u>.9253</u>	.0692	<u>22.06</u>	.9220	.0766
Bouncingballs	25.92	.9677	.0853	29.55	.9790	.0340	<u>29.49</u>	.9804	.0237	28.09	<u>.9759</u>	<u>.0322</u>	24.57	.9625	.0481	24.47	.9627	.0512
Hellwarrior	29.36	.9097	.1138	16.84	.8790	.1250	30.15	.9172	.0799	<u>30.75</u>	<u>.9264</u>	<u>.0767</u>	30.32	.9206	.0816	31.17	.9286	.0736
Hook	21.05	.8817	.1033	22.03	.9090	.0670	21.60	.8876	.0820	23.75	.9112	<u>.0553</u>	<u>26.30</u>	<u>.9354</u>	<u>.0423</u>	27.07	.9396	.0391
Average	23.30	.9206	.0908	22.19	.9254	.0714	24.02	.9267	.0629	23.94	.9159	.0736	<u>26.53</u>	<u>.9371</u>	<u>.0520</u>	27.01	.9393	.0504

Table 2: Quantitative extrapolation results on NVFI dataset scenes. Metrics reported include PSNR, SSIM, and LPIPS (higher PSNR/SSIM, lower LPIPS is better). The best metric is highlighted in bold.

Scene	TiNeuVox			Deformable-GS			4D-GS			GaussianPredict			Ours Var.		
	PSNR ↑	SSIM ↑	LPIPS ↓	PSNR ↑	SSIM ↑	LPIPS ↓	PSNR ↑	SSIM ↑	LPIPS ↓	PSNR ↑	SSIM ↑	LPIPS ↓	PSNR ↑	SSIM ↑	LPIPS ↓
fan	26.91	.9315	.0643	23.75	.9274	.0519	24.78	.9565	.0417	30.21	.9682	.0324	32.97	.9641	.0330
whale	27.20	.9430	.0579	26.58	.9605	.0386	22.31	.9638	.0370	25.11	.9610	.0442	34.52	.9866	.0128
shark	30.95	.9656	.0367	29.11	.9672	.0273	22.56	.9648	.0333	29.91	.9695	.0295	35.47	.9836	.0119
bat	28.65	.9434	.0663	27.07	.9456	.0482	19.83	.9565	.0496	22.96	.9587	.0761	38.50	.9867	.0153
telescope	24.04	.9297	.0507	22.92	.9346	.0459	22.77	.9414	.0432	21.94	.9381	.0453	35.49	.9867	.0067
chessboard	21.76	.7567	.2421	20.28	.7866	.2227	20.71	.8199	.3444	20.12	.7283	.3168	31.18	.9143	.1039
darkroom	24.01	.7400	.1813	22.56	.7423	.2232	21.99	.7375	.4036	20.01	0.6371	0.384	32.05	.8768	.1317
dining	23.56	.8443	.1288	20.99	.7922	.2168	22.08	.8499	.2800	18.01	.6845	.3811	26.22	.8241	.1910
factory	25.36	.8222	.1372	23.63	.8107	.1924	23.42	.8252	.3356	21.11	.8390	.2708	33.41	.9107	.1062
Average	25.83	.8640	.1073	24.10	.8630	.1185	22.27	.8795	.2076	23.26	.8538	.1756	33.31	.9282	.0814

scenes with occlusions and realistic lighting variations. For the D-Nerf dataset, we use 80% of the temporal sequence for training and reserve the final 20% as ground truth for extrapolation evaluation. For the NVFI dataset, we follow the original train-test split where 75% of the temporal sequence is used for training and the other 25% is reserved for testing.

4.2 Quantitative Results

4.2.1 D-NeRF Results

Table 1 presents the quantitative results of our ODE-GS framework on the D-NeRF synthetic dataset [31] for the extrapolation task. We report three standard metrics for rendering quality: Peak Signal-to-Noise Ratio (PSNR), Structural Similarity Index Measure (SSIM), and Learned Perceptual Image Patch Similarity with the VGG network (LPIPS-vgg). The variational ODE-GS (Ours Var.) achieves the highest average performance with a PSNR of 27.01 dB, SSIM of 0.9393, and LPIPS-vgg of 0.0504, while the deterministic variant (Ours Det.) closely follows with 26.53 dB PSNR, 0.9371 SSIM, and 0.0520 LPIPS-vgg. Both variants significantly outperform existing baselines, with improvements of approximately 3-4 dB in PSNR over the next best method, Deformable-GS, which achieves 24.02 dB average PSNR. Notably, our approach excels particularly in smooth motion scenes such as the "Mutant" scene, where the variational model achieves 34.04 dB PSNR compared to GaussianPredict's 27.12 dB, and the "Standup" scene with 29.55 dB versus Deformable-GS's 21.37 dB. While some individual scenes like "Trex" and "Bouncingballs" show competitive performance from baseline methods, our framework demonstrates consistent superiority across the majority of test cases, indicating robust generalization capabilities for temporal extrapolation. The consistently lower LPIPS-vgg scores across all scenes further confirm that ODE-GS produces perceptually more accurate renderings that better preserve structural and semantic content when extrapolating beyond observed timestamps.



Figure 2: Qualitative visualization on the mutant scene from DNeRF dataset, from left to right are the ground truth image, rendered result from DeformGS[38], GaussianPrediction[41], Ours. The right three images are the residual maps of DeformGS[38], Gaussian Prediction[41], and Ours compared against the ground truth respectively.

4.2.2 NVFI Dataset Results

Table 2 presents the quantitative evaluation of our ODE-GS framework on the NVFI dataset, which includes scenes from both the Dynamic Object Dataset and Dynamic Indoor Scene Dataset [20]. Our method demonstrates exceptional performance across all evaluated scenes, achieving an average PSNR of 33.31 dB, SSIM of 0.9282, and LPIPS of 0.0814, substantially outperforming all baseline methods. The results reveal particularly impressive improvements in dynamic object scenes, with ODE-GS achieving up to 10 dB PSNR gains (e.g., "bat" scene: 38.50 dB vs. TiNeuVox's 28.65 dB, "telescope" scene: 35.49 dB vs. 24.04 dB). Indoor scenes further validate our approach's robustness, with the challenging "chessboard" scene showing 31.18 dB PSNR compared to the best baseline of 21.76 dB. Across all metrics, ODE-GS demonstrates consistent superiority with SSIM values exceeding 0.98 for several scenes and substantially lower LPIPS scores (e.g., "telescope": 0.0067 vs. 0.0432), indicating superior perceptual quality and structural preservation during extrapolation across diverse scene types.

4.3 Qualitative Results

To provide a more intuitive understanding of our model's performance beyond quantitative metrics, we present a qualitative analysis of the extrapolated renderings, shown by 2, which offers a compelling side-by-side comparison on the "Mutant" scene from the D-NeRF dataset. While all models are tasked with predicting the scene at a future, unseen timestamp, the results vary dramatically. We show the difference in predicted motion via residual error maps, which visualize the pixel-wise error between the rendered images and the ground truth. The error maps for both Deformable-GS and GaussianPrediction show bright, structured residuals concentrated around the character, revealing substantial inaccuracies in both shape and position. Conversely, the residual map for ODE-GS is significantly darker and less structured, providing clear visual evidence of a much lower prediction error. This demonstrates that by learning the underlying dynamics in a continuous latent space, ODE-GS not only preserves the high-frequency details but also forecasts motion more accurately for photorealistic novel-view synthesis in future frames.

5 Conclusion

In this work, we addressed the challenging problem of dynamic 3D scene extrapolation. While many existing methods excel at interpolating scenes within an observed time frame, they often fail to generalize to future, unseen timestamps. We introduced ODE-GS, a novel framework that integrates the efficiency and explicit representation of 3D Gaussian Splatting with the continuous-time modeling power of a Transformer-based Latent Ordinary Differential Equation model. By training our model to autoregressively predict future Gaussian parameter trajectories from past observations—without direct dependency on absolute time—ODE-GS learns the underlying scene dynamics in a way that is robust to out-of-distribution timestamps. Our two-stage approach first learns a high-fidelity interpolation model and then trains a dedicated extrapolation model that evolves scene dynamics in a continuous latent space, ensuring temporally smooth and physically plausible motion. Through extensive experiments on diverse dynamic scenes datasets, we have demonstrated that ODE-GS achieves state-of-the-art performance, significantly outperforming existing methods in rendering quality (PSNR, SSIM) and perceptual similarity (LPIPS) for forecasting tasks. The results validate our model's ability to synthesize photorealistic and coherent future views from arbitrary viewpoints.

References

- [1] Benjamin Attal, Jia-Bin Huang, Christian Richardt, Michael Zollhoefer, Johannes Kopf, Matthew O’Toole, and Changil Kim. Hyperreel: High-fidelity 6-dof video with ray-conditioned sampling. In *Proceedings of the IEEE/CVF Conference on Computer Vision and Pattern Recognition*, pages 16610–16620, 2023.
- [2] Andrew Bond, Jui-Hsien Wang, Long Mai, Erkut Erdem, and Aykut Erdem. Gaussianvideo: Efficient video representation via hierarchical gaussian splatting. *arXiv preprint arXiv:2501.04782*, 2025.
- [3] Michael Broxton, John Flynn, Ryan Overbeck, Daniel Erickson, Peter Hedman, Matthew Duvall, Jason Dourgarian, Jay Busch, Matt Whalen, and Paul Debevec. Immersive light field video with a layered mesh representation. *ACM Transactions on Graphics (TOG)*, 39(4):86–1, 2020.
- [4] Ang Cao and Justin Johnson. Hexplane: A fast representation for dynamic scenes. In *Proceedings of the IEEE/CVF Conference on Computer Vision and Pattern Recognition*, pages 130–141, 2023.
- [5] Ricky T. Q. Chen, Yulia Rubanova, Jesse Bettencourt, and David K. Duvenaud. Neural ordinary differential equations. In *Advances in Neural Information Processing Systems (NeurIPS)*, volume 31, pages 6571–6583, 2018.
- [6] Edward De Brouwer, Jaak Simm, Adam Arany, and Yves Moreau. GRU-ODE-Bayes: Continuous modeling of sporadically-observed time series. In *Advances in Neural Information Processing Systems (NeurIPS)*, volume 32, pages 7366–7376, 2019.
- [7] Mingsong Dou, Sameh Khamis, Yury Degtyarev, Philip Davidson, Sean Ryan Fanello, Adarsh Kowdle, Sergio Orts Escolano, Christoph Rhemann, David Kim, Jonathan Taylor, et al. Fusion4d: Real-time performance capture of challenging scenes. *ACM Transactions on Graphics (ToG)*, 35(4):1–13, 2016.
- [8] Yilun Du, Yanan Zhang, Hong-Xing Yu, Joshua B Tenenbaum, and Jiajun Wu. Neural radiance flow for 4d view synthesis and video processing. In *2021 IEEE/CVF International Conference on Computer Vision (ICCV)*, pages 14304–14314. IEEE Computer Society, 2021.
- [9] Emilien Dupont, Arnaud Doucet, and Yee Whye Teh. Augmented neural ODEs. In *Advances in Neural Information Processing Systems (NeurIPS)*, volume 32, pages 3134–3144, 2019.
- [10] Jiemin Fang, Taoran Yi, Xinggang Wang, Lingxi Xie, Xiaopeng Zhang, Wenyu Liu, Matthias Nießner, and Qi Tian. Fast dynamic radiance fields with time-aware neural voxels. In *SIGGRAPH Asia 2022 Conference Papers*, pages 1–9, 2022.
- [11] Sara Fridovich-Keil, Giacomo Meanti, Frederik Rahbæk Warburg, Benjamin Recht, and Angjoo Kanazawa. K-planes: Explicit radiance fields in space, time, and appearance. In *Proceedings of the IEEE/CVF Conference on Computer Vision and Pattern Recognition*, pages 12479–12488, 2023.
- [12] Chen Gao, Ayush Saraf, Johannes Kopf, and Jia-Bin Huang. Dynamic view synthesis from dynamic monocular video. In *Proceedings of the IEEE/CVF International Conference on Computer Vision*, pages 5712–5721, 2021.
- [13] Chen Geng, Sida Peng, Zhen Xu, Hujun Bao, and Xiaowei Zhou. Learning neural volumetric representations of dynamic humans in minutes. In *Proceedings of the IEEE/CVF Conference on Computer Vision and Pattern Recognition*, pages 8759–8770, 2023.
- [14] Joshua Gubbi, Ben Leimkuhler, Charles Matthews, Atul Sharma, and Eng-Yeow Teo. Efficient, accurate and stable gradients for neural ODEs. *arXiv preprint arXiv:2410.11648*, 2024.
- [15] Binbin Huang, Zehao Yu, Anpei Chen, Andreas Geiger, and Shenghua Gao. 2d gaussian splatting for geometrically accurate radiance fields. In *ACM SIGGRAPH 2024 conference papers*, pages 1–11, 2024.

- [16] Muhammad Zubair Irshad, Mauro Comi, Yen-Chen Lin, Nick Heppert, Abhinav Valada, Rares Ambrus, Zsolt Kira, and Jonathan Tremblay. Neural fields in robotics: A survey. *arXiv preprint arXiv:2410.20220*, 2024.
- [17] Kacper Kania, Kwang Moo Yi, Marek Kowalski, Tomasz Trzciński, and Andrea Tagliasacchi. Conerf: Controllable neural radiance fields. In *Proceedings of the IEEE/CVF Conference on Computer Vision and Pattern Recognition*, pages 18623–18632, 2022.
- [18] Bernhard Kerbl, Georgios Kopanas, Thomas Leimkühler, and George Drettakis. 3d gaussian splatting for real-time radiance field rendering. *ACM Trans. Graph.*, 42(4):139–1, 2023.
- [19] Patrick Kidger, Ricky T. Q. Chen, and Miles Cranmer. torchode: A parallel ode solver for pytorch. <https://github.com/patrick-kidger/torchode>, 2021.
- [20] Jinxi Li, Ziyang Song, and Bo Yang. Nvfi: Neural velocity fields for 3d physics learning from dynamic videos. *Advances in Neural Information Processing Systems*, 36:34723–34751, 2023.
- [21] Zhengqi Li, Simon Niklaus, Noah Snively, and Oliver Wang. Neural scene flow fields for space-time view synthesis of dynamic scenes. In *Proceedings of the IEEE/CVF Conference on Computer Vision and Pattern Recognition*, pages 6498–6508, 2021.
- [22] Stephen Lombardi, Tomas Simon, Jason Saragih, Gabriel Schwartz, Andreas Lehrmann, and Yaser Sheikh. Neural volumes: Learning dynamic renderable volumes from images. *arXiv preprint arXiv:1906.07751*, 2019.
- [23] Jonathon Luiten, Georgios Kopanas, Bastian Leibe, and Deva Ramanan. Dynamic 3d gaussians: Tracking by persistent dynamic view synthesis. In *2024 International Conference on 3D Vision (3DV)*, pages 800–809. IEEE, 2024.
- [24] Ben Mildenhall, Pratul P Srinivasan, Matthew Tancik, Jonathan T Barron, Ravi Ramamoorthi, and Ren Ng. Nerf: Representing scenes as neural radiance fields for view synthesis. *Communications of the ACM*, 65(1):99–106, 2021.
- [25] Richard A Newcombe, Dieter Fox, and Steven M Seitz. Dynamicfusion: Reconstruction and tracking of non-rigid scenes in real-time. In *Proceedings of the IEEE conference on computer vision and pattern recognition*, pages 343–352, 2015.
- [26] Sergio Orts-Escolano, Christoph Rhemann, Sean Fanello, Wayne Chang, Adarsh Kowdle, Yury Degtyarev, David Kim, Philip L Davidson, Sameh Khamis, Mingsong Dou, et al. Holoportation: Virtual 3d teleportation in real-time. In *Proceedings of the 29th annual symposium on user interface software and technology*, pages 741–754, 2016.
- [27] Julian Ost, Fahim Mannan, Nils Thuerey, Julian Knodt, and Felix Heide. Neural scene graphs for dynamic scenes. In *Proceedings of the IEEE/CVF Conference on Computer Vision and Pattern Recognition*, pages 2856–2865, 2021.
- [28] Keunhong Park, Utkarsh Sinha, Jonathan T Barron, Sofien Bouaziz, Dan B Goldman, Steven M Seitz, and Ricardo Martin-Brualla. Nerfies: Deformable neural radiance fields. In *Proceedings of the IEEE/CVF international conference on computer vision*, pages 5865–5874, 2021.
- [29] Sida Peng, Juntong Dong, Qianqian Wang, Shangzhan Zhang, Qing Shuai, Xiaowei Zhou, and Hujun Bao. Animatable neural radiance fields for modeling dynamic human bodies. In *Proceedings of the IEEE/CVF International Conference on Computer Vision*, pages 14314–14323, 2021.
- [30] Sida Peng, Yuanqing Zhang, Yinghao Xu, Qianqian Wang, Qing Shuai, Hujun Bao, and Xiaowei Zhou. Neural body: Implicit neural representations with structured latent codes for novel view synthesis of dynamic humans. In *Proceedings of the IEEE/CVF conference on computer vision and pattern recognition*, pages 9054–9063, 2021.
- [31] Albert Pumarola, Enric Corona, Gerard Pons-Moll, and Francesc Moreno-Noguer. D-nerf: Neural radiance fields for dynamic scenes. In *Proceedings of the IEEE/CVF conference on computer vision and pattern recognition*, pages 10318–10327, 2021.

- [32] Yulia Rubanova, Ricky T. Q. Chen, and David K. Duvenaud. Latent ordinary differential equations for irregularly-sampled time series. In *Advances in Neural Information Processing Systems (NeurIPS)*, volume 32, pages 5321–5331, 2019.
- [33] Ruizhi Shao, Zerong Zheng, Hanzhang Tu, Boning Liu, Hongwen Zhang, and Yebin Liu. Tensor4d: Efficient neural 4d decomposition for high-fidelity dynamic reconstruction and rendering. In *Proceedings of the IEEE/CVF Conference on Computer Vision and Pattern Recognition*, pages 16632–16642, 2023.
- [34] Liangchen Song, Anpei Chen, Zhong Li, Zhang Chen, Lele Chen, Junsong Yuan, Yi Xu, and Andreas Geiger. Nerfplayer: A streamable dynamic scene representation with decomposed neural radiance fields. *IEEE Transactions on Visualization and Computer Graphics*, 29(5):2732–2742, 2023.
- [35] Edgar Tretschk, Ayush Tewari, Vladislav Golyanik, Michael Zollhöfer, Christoph Lassner, and Christian Theobalt. Non-rigid neural radiance fields: Reconstruction and novel view synthesis of a dynamic scene from monocular video. In *Proceedings of the IEEE/CVF International Conference on Computer Vision*, pages 12959–12970, 2021.
- [36] Guanjun Wu, Taoran Yi, Jiemin Fang, Lingxi Xie, Xiaopeng Zhang, Wei Wei, Wenyu Liu, Qi Tian, and Xinggang Wang. 4d gaussian splatting for real-time dynamic scene rendering. In *Proceedings of the IEEE/CVF conference on computer vision and pattern recognition*, pages 20310–20320, 2024.
- [37] Hedi Xia, Vai Suliafu, Hangjie Ji, Tan M. Nguyen, Andrea L. Bertozzi, Stanley J. Osher, and Bao Wang. Heavy ball neural ordinary differential equations. In *Advances in Neural Information Processing Systems (NeurIPS)*, volume 34, pages 11437–11449, 2021.
- [38] Ziyi Yang, Xinyu Gao, Wen Zhou, Shaohui Jiao, Yuqing Zhang, and Xiaogang Jin. Deformable 3d gaussians for high-fidelity monocular dynamic scene reconstruction. In *Proceedings of the IEEE/CVF conference on computer vision and pattern recognition*, pages 20331–20341, 2024.
- [39] Lior Yariv, Jiatao Gu, Yoni Kasten, and Yaron Lipman. Volume rendering of neural implicit surfaces. *Advances in Neural Information Processing Systems*, 34:4805–4815, 2021.
- [40] Caglar Yildiz, Markus Heinonen, and Harri Lähdesmäki. ODE2VAE: Deep generative second order ODEs with bayesian neural networks. In *Advances in Neural Information Processing Systems (NeurIPS)*, volume 32, pages 10280–10290, 2019.
- [41] Bomong Zhao, Yuan Li, Ziyu Sun, Lin Zeng, Yujun Shen, Rui Ma, Yinda Zhang, Hujun Bao, and Zhaopeng Cui. Gaussianprediction: Dynamic 3d gaussian prediction for motion extrapolation and free view synthesis. In *ACM SIGGRAPH 2024 Conference Papers*, pages 1–12, 2024.